3D microperfusion of mesoscale human microphysiological liver models improves functionality and recapitulates hepatic zonation

Wesseler, Milan Finn; Taebnia, Nayere; Harrison, Sean; Youhanna, Sonia; Preiss, Lena C.; Kemas, Aurino M.; Vegvari, Akos; Mokry, Jaroslav; Sullivan, Gareth J.; Lauschke, Volker M.

Total number of authors:
11

Published in:
Acta Biomaterialia

Link to article, DOI:
10.1016/j.actbio.2023.09.022

Publication date:
2023

Document Version
Publisher's PDF, also known as Version of record

Acta Biomaterialia 171 (2023) 336–349

Contents lists available at ScienceDirect

Acta Biomaterialia

journal homepage: www.elsevier.com/locate/actbio

Full length article

3D microperfusion of mesoscale human microphysiological liver models improves functionality and recapitulates hepatic zonation

Milan Finn Wesseler[a,1], Nayere Taebnia[a,1], Sean Harrison[b], Sonia Youhanna[c], Lena C. Preiss[c,d], Aurino M. Kemas[c], Akos Vegvari[e], Jaroslav Mokry[f], Gareth J. Sullivan[b,*], Volker M. Lauschke[c,g,h,*], Niels B. Larsen[a,*]

[a] Department of Health Technology, DTU Health Tech, Technical University of Denmark, Kgs, Lyngby, Denmark
[b] Department of Pediatric Research, Oslo University Hospital, Oslo, Norway
[c] Department of Physiology and Pharmacology, Karolinska Institutet, Stockholm, Sweden
[d] Department of Drug Metabolism and Pharmacokinetics (DMPK), the healthcare business of Merck KGaA, Darmstadt, Germany
[e] Department of Medical Biochemistry and Biophysics, Karolinska Institutet, Stockholm, Sweden
[f] Department of Histology and Embryology, Faculty of Medicine in Hradec Králové, Charles University, Hradec, Králové, Czech Republic
[g] Dr Margarete Fischer-Bosch Institute of Clinical Pharmacology, Stuttgart, Germany
[h] University of Tübingen, Tübingen, Germany

ARTICLE INFO

Article history:
Received 22 February 2023
Revised 26 August 2023
Accepted 14 September 2023
Available online 19 September 2023

Keywords:
Microperfusion
Liver models
Stereolithography
Primary human hepatocytes
Induced pluripotent stem cells
Zonation

ABSTRACT

Hepatic *in vitro* models that accurately replicate phenotypes and functionality of the human liver are needed for applications in toxicology, pharmacology and biomedicine. Notably, it has become clear that liver function can only be sustained in 3D culture systems at physiologically relevant cell densities. Additionally, drug metabolism and drug-induced cellular toxicity often follow distinct spatial micropatterns of the metabolic zones in the liver acinus, calling for models that capture this zonation. We demonstrate the manufacture of accurate liver microphysiological systems (MPS) via engineering of 3D stereolithography printed hydrogel chips with arrays of diffusion open synthetic vasculature channels at spacings approaching *in vivo* capillary distances. Chip designs are compatible with seeding of cell suspensions or preformed liver cell spheroids. Importantly, primary human hepatocytes (PHH) and hiPSC-derived hepatocyte-like cells remain viable, exhibit improved molecular phenotypes compared to isogenic monolayer and static spheroid cultures and form interconnected tissue structures over the course of multiple weeks in perfused culture. 3D optical oxygen mapping of embedded sensor beads shows that the liver MPS recapitulates oxygen gradients found in the acini, which translates into zone-specific acet-ami-no-phen toxicity patterns. Zonation, here naturally generated by high cell densities and associated oxygen and nutrient utilization along the flow path, is also documented by spatial proteomics showing increased concentration of periportal- *versus* perivenous-associated proteins at the inlet region and *vice versa* at the outlet region. The presented microperfused liver MPS provides a promising platform for the mesoscale culture of human liver cells at phenotypically relevant densities and oxygen exposures.

Statement of significance

A full 3D tissue culture platform is presented, enabled by massively parallel arrays of high-resolution 3D printed microperfusion hydrogel channels that functionally mimics tissue vasculature. The platform supports long-term culture of liver models with dimensions of several millimeters at physiologically relevant cell densities, which is difficult to achieve with other methods. Human liver models are generated from seeded primary human hepatocytes (PHHs) cultured for two weeks, and from seeded spheroids of hiPSC-derived human liver-like cells cultured for two months. Both model types show improved functionality over state-of-the-art 3D spheroid suspensions cultured in parallel. The platform can generate physiologically relevant oxygen gradients driven by consumption rather than supply, which was validated by

* Corresponding authors.
E-mail addresses: gareth.sullivan@medisin.uio.no (G.J. Sullivan), volker.lauschke@ki.se (V.M. Lauschke), nibl@dtu.dk (N.B. Larsen).
[1] Shared first authors

https://doi.org/10.1016/j.actbio.2023.09.022

visualization of embedded oxygen-sensitive microbeads, which is exploited to demonstrate zonation-specific toxicity in PHH liver models.

1. Introduction

3D *in vitro* cell culture models have become increasingly prevalent for research in toxicology, pharmacology and disease modeling [1]. The liver is among the tissues for which transitioning from conventional monolayer cultures to organotypic 3D models has arguably the largest impact. Even though 2D adhesion cultures are a robust, easy-to-use, and high-throughput compatible research tool, rapid dedifferentiation of seeded primary hepatocytes within hours limits their utility to short-term experiments [2,3]. An increasing number of applications require liver cultures that are functionally stable for multiple days to weeks. Examples are i) clearance predictions of drug candidates with low metabolic turnover, which are increasingly common in drug discovery, ii) evaluations of chronic hepatotoxicity, which constitute the majority of clinically observed idiosyncratic liver injury cases, and iii) screening of compounds in models of chronic liver disease to identify novel candidate drugs.

Advanced 3D human hepatocyte culture models presented in recent years improve the maintenance of the organotypic microenvironment, including multicellular spheroids and microphysiological systems (MPS) [4–9]. Spheroid culture formats are reasonably easy to use, reproducible, allow medium to high throughput screening, and have shown vast improvements in retention of mature phenotypes compared to 2D adhesion cultures [10]. However, spheroids do not recapitulate hepatic zonation that is important for the study of zone-specific drug toxicities and interzonal interactions. This is likely due to the inability of static culture to establish and maintain oxygen gradients present in liver tissue *in vivo*, which range from ≈50 mmHg in periportal tissue to ≈20 mmHg in perivenous tissue of the liver acinus [11]. Consequently, zonation requires more complex perfused liver systems that allow for the controlled establishment and maintenance of physiologically relevant gradients in oxygen tension.

Hepatic zonation has been pursued in reported models of 2D static cultures at different oxygen tensions [12,13], 2D flow-over cultures [14,15], and 3D flow-through cultures based on 3D printed scaffolds [16] and bundled cell-laden microfibers [17]. Flow-over and flow-through perfusion models provide close contact and consequently highly efficient gas- and nutrient-exchange with cells in direct contact with the perfusion liquid. However, the flowing liquid also exerts super-physiological levels of shear stress and may prevent the establishment of local tissue concentration gradients present *in vivo*. Model cell types have mainly been liver cell lines, as well as primary rodent and human hepatocytes. While these different culture format approaches are promising and have modeled important expression and secretory characteristics of liver tissue, no model with physiological oxygen gradients along the perfusion axis of a continuous and densely perfused 3D tissue has been reported.

Here, we present a mesoscale culture system of 3D interconnected liver tissue at physiological cell densities supporting oxygen gradients resembling those in the liver acinus *in vivo* (*Fig. 1*). We developed an MPS with synthetic vasculature arrays that traverse cell culture cavities with spacings that resemble physiological inter-capillary distances. The MPS is mounted in a custom designed microscopy-compatible table-top incubator with temperature and gas control as well as heated glasses for condensation-free optical access, ensuring robust tubing connection in a controlled and aseptic environment that can be monitored during long-term culture. The synthetic vasculature arrays are 3D printed in a mechanically stable yet diffusion-open hydrogel that can be directly connected to external perfusion tubing. The MPS design enables longitudinal imaging of the entire replicated liver acinus *in situ* and supports live oxygen mapping based on embedded microsensor beads to monitor the establishment and maintenance of physiological oxygen gradients, which translate into zone-specific functional differences. Primary human hepatocytes (PHH) and human induced pluripotent stem cell-derived hepatocyte-like cells (HLC) cultured for two weeks and two months, respectively, remain metabolically active, and PHH cultures remain responsive to inducers of nuclear hormone receptor signaling, and sensitive to hepatotoxins with a zone-specific toxicity pattern. Furthermore, we demonstrate phenotypic improvements compared to isogenic cultures in 2D and static 3D spheroid cultures, indicating that increased cell density and massively parallel microperfusion synergize to further enhance liver cell phenotypes.

2. Materials and methods

2.1. 3D liver MPS design, printing, and sterilization

The hydrogel-based 3D liver MPS was designed using CAD software (Inventor Professional 2018, Autodesk). The custom-build stereolithographic hydrogel printer along with cytotoxicity assessment of printing resins have been presented in our previous work [18]. The optimized pre-polymer solution used here consisted of 180 mg mL^{-1} poly(ethylene glycol) diacrylate (PEGDA; M_n 700 g mol^{-1}; Sigma-Aldrich), 20 mg mL^{-1} poly(ethylene glycol) diacrylate (PEGDA; M_n 5000 g mol^{-1}; Creative PEGWorks), 11.25 mg mL^{-1} quinoline yellow (Sigma-Aldrich), 5 mg mL^{-1} lithium phenyl-2,4,6-trimethylbenzoylphosphinate (LAP, Sigma-Aldrich) in water. Printing used an exposure time of 4.5 s (luminous flux of 14 mW cm^{-2} at 365 nm) per printed layer with a step height of 20 µm. The printing time was 90 min per chip. The pre-polymer solution was passed through a 0.22 µm pore size filter before printing to remove any particulates. The final prints were immersed in 2.5% glutaraldehyde in PBS (G6257, Sigma-Aldrich) for 48 h followed by immersion in 70% ethanol for 24 h, both at room temperature. The solution exchange was performed in a fume hood due to the toxicity of glutaraldehyde. Following glutaraldehyde and ethanol sterilization, sample containers were only opened in LAF benches to ensure sterility. Samples were incubated four times 12 h in fresh PBS to remove residual sterilization reagents and printing solution components. As the final step, chips were incubated in complete cell culture medium for the targeted culture application for 6 h to avoid medium component dilution into the print material on cell seeding. The developed post-printing sterilization protocol reliably prevented contamination stemming from imprinted bacteria while avoiding damage to the structure of the hydrogel chips. Without addition of high molecular weight monomer (PEGDA M_n 5000 g mol^{-1}), immersion in 70% ethanol caused crack formation. Sterilization by heat or hydrogen peroxide treatments led to crack formation with all investigated resin formulations.

2.2. Incubation system for long-term cell culture and in situ imaging

An MPS holder system was developed to facilitate stable fluidic connection of the MPS and its perfusion tubing and to

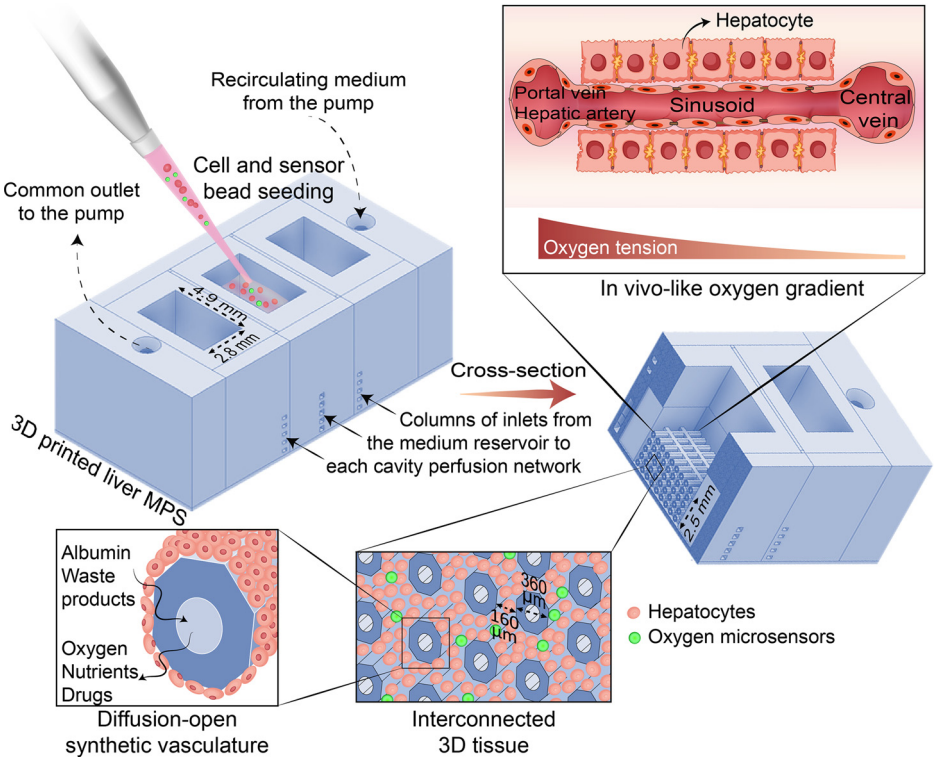

Fig. 1. Schematic of the liver MPS hydrogel chip. Cells or spheroids are seeded by pipetting directly into each of the three culture cavities, without or with addition of oxygen sensor beads. The immersed 3D printed chip is perfused in a simple loop between the inlet and outlet, with the surrounding medium functioning as reservoir. A cross-sectional view through the center cavity of the liver model acinus cavity shows the 2D array of synthetic vasculature channels that enable the establishment of oxygen tension gradients mimicking the *in vivo* situation. The hydrogel channels allow for diffusion of supplied oxygen, nutrients, and drugs as well as collection of cell products such as albumin and cellular waste, while shielding cultured cells from shear forces of the perfusion medium.

ensure sterility, limit evaporation, and ease handling during seeding and medium exchange. The holder system was designed using CAD software (Inventor Professional 2018) and printed with a Form 3B stereolithographic printer in Dental LT resin (both Formlabs). Post-processing to ensure cytocompatibility consisted of 3 steps, comprising 15 min wash in isopropanol (34,863, Sigma-Aldrich) in a FormWash sonicator bath (Formlabs), two times 1 h immersion in isopropanol on a shaker plate at 50 rpm, and three times immersion in deionized water for 48 h. Holders were sterilized by wiping the outer surfaces with 70% ethanol and subsequent UV-C exposure for 30 min on each side using a UV sterilization box (Clean View UV Cabinet, Cleaver Scientific) inside a LAF bench. Custom-built incubators compatible with mounting on a microscope stage and with heated top and bottom glasses, controlled gas supply, and integrated heaters and temperature sensors were used for long-term culture of MPS's mounted in the holder system. Each incubator was supplied by a gas flow of 30 µL min^{-1} of premixed 95% air/5% CO_2 using mass flow controllers (type 1179A, MKS) passed through a 0.22 µm membrane filter (Q-Max Syringe Filter, Frisenette). Incubators and holders were sterilized by wiping their outer surfaces thoroughly with 70% ethanol and exposure to UV-C for 30 min on all sides. A closed perfusion tube loop was assembled from Santoprene® tubing (GPR-0051–008, Advanced Elastomer Systems) with inner diameter 0.51 mm in combination with pump stopper tubing (Pharmed BPT SC0731, Ismatec, Cole-Palmer) and custom cut 21 G stainless steel needles of 30 mm length (Adhesive Dispensing). The closed tubing loop driven by a peristaltic pump passes the incubator wall via a 3D printed tube guide. The perfusion rate was set to 120 µL min^{-1} unless indicated otherwise for specific experiments. Assembled tubing loops were sterilized by flushing 70% ethanol followed by PBS and autoclaved at 121 °C for 15 min. The incubator created an aseptic, sealed environment with interfacing for heating controllers, gas supply and perfusion tubing. Heated top and bottom glasses allowed for microscopy throughout long-term culture periods by ensuring temperature stability across the culture volume and preventing water condensation that would compromise visual access. The temperature was monitored to be 35.5–37.0 °C during long-term culture.

2.3. Oxygen sensor integration and co-localized live cell 3D oxygen mapping

The experimental procedure for bead coating, co-localized live-cell and oxygen mapping as well as signal processing of the CPOx-50-PtP is described in detail in our previous work [19]. Briefly, oxygen sensor beads are integrated into 3D cell cultures, parallel fluorescence and phosphorescence lifetime images are acquired using a confocal FLIM/PLIM DCS-120 (Becker & Hickl) unit connected to an Axio Observer Z1 (Carl Zeiss) with Fluar 5x/0.25NA (WD 12.5 mm) and LD Plan Neofluar 20x/0.4NA (WD 8.9 mm) objectives. The acquired data is processed using a custom-made image analysis program [19]. For the liver MPS systems, 3 µL of 5 mg mL^{-1} platinum-porphin based oxygen sensor beads CPOx-50-PtP (Colibri Photonics) were added to each cavity before seeding the cells. In addition, oxygen sensor beads were added to the cell suspensions of all cell types at a concentration of 0.25 mg mL^{-1}. The commercially available sensor beads have previously been employed in numerous cell culture studies without indications of affecting cell behavior [20]. As a further precaution, confocal imaging to assess the oxygen distribution was only performed intermittantly to minimize the risk of analysis-induced effects on the cultured cells.

2.4. Liver cell line maintenance and MPS culture

Hep G2 hepatocellular carcinoma cells (85,011,430, ECACC, UK) were cultured in complete medium consisting of EMEM (EBSS) supplemented with 2 mM glutamine (L-glutamine solution, CAS No. 56–85–9, BioXtra; G7513, Sigma-Alrich), 1% non-essential amino acids (MEM Non-essential amino acid solution, BioReagent; M7145, Sigma-Aldrich), 10% v/v FBS (S1810, Biowest) and 1% v/v penicillin-streptomycin (Sigma-Aldrich). Cells were maintained in T175 culture flasks at 37 °C and 5% CO_2. Medium was exchanged every 3–4 days and cells were passaged upon 80% confluency. Cells were used between passage 5 and 19 for liver MPS experiments. Hep G2 were seeded at approximately 4×10^6 cells per liver MPS cavity by preparing a suspension of 56×10^6 cells mL^{-1} (containing oxygen sensor beads as described above) and seeding 70 µL of cell suspension per cavity. Gentle pipetting was used to populate voids around 3D channel arrays. During perfusion culture, medium was exchanged every 2 days.

2.5. Stem cell differentiation and culture

Differentiation of human iPSC-derived hepatocyte-like spheroids in suspension culture was performed as described previously [21]. On day 6 of differentiation, spheroids were shipped for seeding. Approximately 50 µL of spheroid mass, as measured if spun down, were seeded per cavity. Spheroids were seeded into the liver MPS and the voids around the synthetic vasculature channel arrays were populated using gentle pipetting and sedimentation. Medium exchange was performed every third day using complete medium composition [21]. Oxygen microsensor bead integration was performed as described above. Live staining was performed by perfusion with 1 µg mL^{-1} calcein acetoxymethyl ester (calcein AM) (Invitrogen eBioscience, Thermo Fisher) in complete medium.

2.6. Primary human hepatocyte culture

Primary human cryoplateable hepatocytes (PHHs; BioIVT) were seeded at approximately 1.0×10^6 cells per liver MPS cavity. In brief, PHHs were thawed in a 37 °C water bath, immersed in 5 mL of pre-warmed InVitroGro CP medium (BioIVT) with 1% Torpedo antibiotic mix (BioIVT), counted and diluted to approximately 14×10^6 cells mL^{-1} in William's E Medium (A1217601, Thermo Fisher) with 10% exosome-depleted FBS (A2720803, Thermo Fisher). Then, 70 µL of cell suspension was seeded into each chip cavity and pipetted carefully to populate voids around the 3D channel array. For the first 6 days of culture, medium with FBS was used, after which consecutive medium exchanges were done with FBS-free medium [22].

2.7. Assessment of metabolic activity

For the assessment of metabolic activity of liver MPS, a previously described assay was applied [23]. Briefly, primary liver MPS samples with or without 72 h prior induction with 10 µM rifampicin (Sigma-Aldrich) in complete medium were incubated in metabolic assay solution containing 10 µM amodiaquine (A7299, Merck) and 10 µM midazolam (midazolam hydrochloride, B. Braun). Samples were taken directly from the recirculating medium in the perfusion tubing after 4 h, 6 h, 8 h, and 10 h and quenched in acetonitrile containing internal standard (Pruvanserin). Concentration of downstream metabolites *N*-desethylamodiaquine and 1′-OH-midazolam formed by CYP2C8 and CYP3A4 respectively were measured using LC-MS/MS. Analysis was performed using an AB Sciex API 6500+ triple quadrupole (AB Sciex LLC) coupled with a Waters Acquity I-Class UPLC (Waters Corporation). Electrospray ionization in positive mode with multiple reaction monitoring was used and data processing was performed with Analyst software (Version 1.7, AB Sciex LLC). Detailed information about parameter settings and analytical column and gradient can be found in Supplementary Table S1 and S2.

2.8. Hepatotoxicity assessment

Liver MPS were exposed from day 8 and for 7 days with acetaminophen (Merck, Germany). On day 15 of culture, cells were stained with 1 µg mL^{-1} calcein AM and 1 µg mL^{-1} propidium iodide (Invitrogen, Thermo Fisher). Fluorescence from the liver MPS was visualized with an AxioObserver Z1 with confocal microscope unit LSM 700 (Carl Zeiss). Image processing to quantify the metabolic activity as a function of axial distance from the inlet side of each MPS was done using Fiji [24]. In brief, a region-of-interest (ROI) covering tissue regions parallel and perpendicular to the channel orientation was defined using the ROI Manager. The resulting combined ROI was converted to an image mask used for applying a boolean "AND" operation on the green and red channels separately. Next, horizontal line profiles averaging the entire mask height were extracted from the green and red channels, as well as for the mask itself, using the Profile tool. Lastly, the green and red intensity profiles were normalized to the extracted mask intensity profile to compensate for the varying number of pixels in the vertical dimension contributing to the averaged fluorescence intensity. Averaging with a rolling window width of 100 µm was applied to the normalized green and red intensity profiles.

2.9. qRT-PCR analysis of tissues

Total RNA was isolated from each chamber of the chips by means of QIAzol lysis treatment followed by reverse transcription of 100–200 ng into cDNA using SuperScript III reverse transcriptase (Invitrogen). Expression levels were analyzed on a 7500 Fast Real-Time PCR system (Applied Biosystems) by qPCR using TaqMan probes (Table S1). Expression levels were calculated using the $\Delta\Delta$Ct method with GAPDH as the housekeeping gene.

2.10. Proteomic analysis of cells

Cell pellets (obtained by collecting cells from the inlet and outlet of the chips) were lysed in 10 µL of 8 M urea and 40 µL of 0.2% ProteaseMAX™ surfactant (Promega) in 20% acetonitrile (ACN) and 100 mM Tris–HCl, pH 8.5, and supplemented with 0.8 µL protease inhibitor cocktail (Pierce) before sonication in water bath for 10 min. Following addition of 29.2 µL of 50 mM Tris–HCl, the samples were sonicated using VibraCell probe (Sonics & Materials, Inc.) for 25 s with pulse 2/2 s (on/off), at 20% amplitude. Lysates were spun down at 12,000 rpm at 4 °C for 10 min. Proteins were reduced by adding 3 µL of 250 mM dithiothreitol (Sigma) and incubated at 37 °C for 45 min and alkylated with addition of 4 µL of 500 mM iodoacetamide (Sigma) at room temperature for 30 min in the dark. Then 0.2 µg of sequencing grade modified trypsin (Promega) was added to the samples and incubated for 16 h at 37 °C. The sample was cleaned on a C18 Hypersep plate with 5–7 µL bed volume (Thermo Fisher Scientific), dried using a vacuum concentrator (Eppendorf) and resuspended in 11 µL of 50 mM TEAB and labeled with TMTpro-18plex mass tag reagent kit (Thermo Fisher Scientific) adding 20 µg reagent in 4.5 µL ACN in a scrambled order and incubated at RT for 2 h. The reaction was stopped by addition of hydroxylamine to a final concentration of 0.5% and incubation at RT for 15 min before samples were combined and cleaned on a C-18 HyperSep plate with 40 µL bed volume (Thermo Fisher Scientific).

TMTpro-labeled peptides were reconstituted in solvent A (0.1% FA, 2% ACN in water) and approximately 2 µg samples injected on a 50 cm long EASY-Spray C18 column (Thermo Fisher Scientific) connected to an Ultimate 3000 nanoUPLC system (Thermo Fisher Scientific) using a 120 min long gradient: 4–26% of solvent B (0.1% FA in 98% ACN) in 120 min, 26–95% in 5 min, and 95% of solvent B for 5 min at a flow rate of 300 nL/min. Mass spectra were acquired on a Q Exactive HF Hybrid Quadrupole-Orbitrap mass spectrometer (Thermo Fisher Scientific) ranging from *m/z* 375 to 1700 at a resolution of $R = 120{,}000$ (at *m/z* 200) targeting 1×10^6 ions for a maximum injection time of 80 ms, followed by data-dependent higher-energy collisional dissociation (HCD) fragmentations of the top 18 precursor ions with a charge state 2+ to 7+, using 45 s dynamic exclusion. The tandem mass spectra were acquired with a resolution of $R = 60{,}000$, targeting 2×10^5 ions for maximum injection time of 54 ms, setting quadrupole isolation width to 1.4 Th and normalized collision energy to 34%.

Acquired raw data files were analyzed in Proteome Discoverer v3.0 (Thermo Fisher Scientific) with MS Amanda v2.0 search engine against human protein database (UniProt, 20,330 consensus entries downloaded on 9 February 2023). A maximum of two missed cleavage sites were allowed for full tryptic digestion, while setting the precursor and the fragment ion mass tolerance to 10 ppm and 0.02, respectively. Carbamidomethylation of cysteine was specified as a fixed modification. Oxidation on methionine, deamidation of asparagine and glutamine as well as TMTpro (+304.207 Da) were set as dynamic modifications. Initial search results were filtered with 5% FDR using Percolator node in Proteome Discoverer. Quantification was based on the precursor ion intensities. Significantly enriched pathways were identified based on the KEGG Pathway Database using the WebGestalt toolbox [25].

2.11. Histology and immunostaining

Tissues were fixed in 4% paraformaldehyde for 4 h, and after washing and dehydration they were embedded in paraffin. 5-µm paraffin-embedded sections were deparaffinized, rehydrated and stained with hematoxylin-eosin (H&E). Prior to immunostaining antigen retrieval was performed in HistoStation (Milestone, Italy). Endogenous peroxidase was blocked in 5% hydrogen peroxide (3 × 10 min) and then, sections were incubated with primary rabbit anti-human albumin (DAKO, Denmark) or mouse anti-human cytokeratin 18, clone DC 10 (DAKO, Denmark) or primary mouse anti-cytokeratin 19, clone BA 17 (DAKO, Denmark; 1:50) antibody for 1 h at room temperature. After washing the sections were exposed to anti-rabbit or anti-mouse DAKO EnVision+ System-HRP Labeled Polymer (DAKO, Denmark) for 35 min at room temperature. Then the reaction was developed with 3,3-diaminobenzidine tetrahydrochloride (Sigma-Aldrich). Sections were dehydrated, counterstained with hematoxylin and mounted in DPX (Sigma-Aldrich). Tissue sections were examined in Olympus BX51 microscope equipped with DP71 camera.

2.12. Albumin secretion analysis

Supernatant was collected from the bioreactor as well as from the 2D cultures at time points throughout the culture period. Supernatant was immediately frozen at −80 °C until analysis. Albumin levels were quantified using a commercially available ELISA kit (E80–129, Fortis Life Sciences) and following the manufacturer's instructions. Briefly, all samples measured in duplicate were diluted 1:50 or 1:100 in sample buffer. 100 µL of samples or standards were added to wells previously coated with the capture antibody (A80–129A). After 1 h incubation, wells were washed 5x with the washing buffer and 100 µL of HRP-conjugated reporting antibody (A80–129P) was added for 1 h incubation. Afterwards, wells were washed as previously before adding 100 µL of TMB substrate for 15 min incubation in the dark. At the end, 100 µL of the stop solution was added and absorbance was measured at 450 nm. Albumin concentration was interpolated from the plotted standard curve.

2.13. Statistical analysis

Results are presented as mean ± SEM unless stated otherwise. To determine statistical significance, unpaired two-tailed heteroscedastic t-tests were performed using GraphPad Prism (version 10.0.2) with $n \geq 3$ samples per group. All data are shown, and no outlier removal was performed. For all data, significance was defined as $p \leq 0.05$.

3. Results

3.1. 3D printed liver MPS hydrogel culture chips

Chips for the liver tissue models were fabricated with a custom-built projection stereolithographic 3D printer [18] using an optimized pre-polymer formulation containing a combination of two monomers of different average molecular weights, namely 180 mg mL^{-1} poly(ethylene glycol) diacrylate (PEGDA) M_n 700 g mol^{-1} and 20 mg mL^{-1} PEGDA M_n 5000 g mol^{-1}. This optimized formulation yielded stable hydrogel culture chips with reliable connections to microperfusion tubing through direct needle insertion. Printing using only low molecular weight PEGDA was found to result in occasional material fracture on repeated needle insertion. The devices could withstand swelling and deswelling without damage during sterilization with 70% ethanol and 2.5% glutaraldehyde, and during cell seeding where the hydrogel chips are taken out of their immersion fluid for up to three hours.

The primary function of the liver MPS chips is to supply high cell density 3D tissues with nutrients and to provide spatially engineered oxygen microenvironments resembling the oxygen gradient present in the human liver acinus *in vivo*. To this end, the MPS was designed to allow for culture of human liver cells at a density of >100 million cells mL^{-1} enabled by perfusion through synthetic diffusion-open vasculature channels (Figure 1; Supplementary Figure S1 and Table S4). The printed chip contains three separate cavities mimicking parallel liver acini, each traversed by 45 synthetic vasculature channels. Each cavity volume is 41 µL with a microchannel-traversed tissue volume of 20 µL, *i.e.*, excluding the volume of channels and channel support structures. Each channel of octagonal cross-section has a designed wall thickness of 100 µm and channel width of 160 µm. Cross-sectional analysis of printed devices shows that slight overcuring in the channel lumen results in equal channel width and wall thickness of 120 µm. The design featured an inter-channel distance of 160 µm, giving a maximum distance from any point inside the tissue to the synthetic vasculature of 190 µm, thereby balancing tissue density and cell-cell connections with diffusion distance. For the seeding of spheroids, channel spacings were adjusted to 440 µm to support efficient sedimentation of pre-formed cellular aggregates with a diameter up to 350 µm. The printing material was chosen to minimize non-specific cell binding and exhibits very low cytotoxicity after thorough post-printing washing [18]. The bottom of each cavity consists of a 200 µm thick layer of printed material with sufficiently low light scattering to allow for high quality optical imaging.

We integrated three parallel cell culture cavities per chip to increase throughput. Uniform perfusion rates of the synthetic vasculature in the three parallel cavities through one common outlet was achieved by fine tuning feeding channel dimensions. With one common outlet, the flow speed in each parallel cavity is determined by the sum of resistances in the inlet feeding channel, the

main cavity, and the outlet feeding channel with the total resistance being influenced by both channel length and cross-sectional diameter. As channel length was impractical to change in the overall chip design, we achieved flow equilibration in the parallel cavities of strongly differing feeding channel lengths by tuning feeding channel cross-sections. In addition, homogenous perfusion through all parallel synthetic vasculature channels was enabled for single feeding inlet and outlet cavities, by introducing perpendicular inlet and outlet feeding channels on opposite sides of the chip. Using these design principles, the device achieved deviations <10% in average flow velocities, as determined by tracking of suspended fluorescent microparticles (Figure S2).

We immersed each liver MPS hydrogel chips in a well of a 6-well plate containing cell culture medium. The inlets to each culture cavity were open to and fed by the surrounding medium in the well. Medium was removed through the common outlet using a peristaltic pump and fed back to the reservoir via the inlet. This enabled perfusion of the chips with pre-conditioned culture medium and efficiently prevented bubbles from being introduced and trapped in the synthetic vasculature networks during long-term culture. In addition, this enabled a decoupling of cell culture medium between chips and thus the application of assays with different conditions for each chip.

3.2. Liver MPS perfusion and incubation platform

To enable the longitudinal profiling of aseptic long-term culture of human liver models under perfusion and controlled gas and temperature microenvironments, we integrated the MPS with custom designed holder systems and a surrounding microscopy-compatible incubator (Fig. 2). The individual holders facilitated the stable handling of the chips after seeding, acted as guides for needle insertion for connection to the perfusion setup, contributed to the shielding of the wells against evaporation and contamination, and allowed for individual removal of MPS chips for analysis. Six of the small liver model holders fit into a larger holder system that kept chips in place for microscopy. Medium exchanges could be performed by lifting the large holder containing the six individual holder units onto a new 6-well-plate containing pre-warmed medium. This holder combination enables stable perfusion with frequent medium exchanges in long-term cell cultures, performed for up to two months in the HLC spheroid culture study, as detailed below. Additionally, this setup including large cell numbers and medium volumes allowed for accessible and regular sampling from the same liver MPS without altering the stoichiometry between medium to cell volumes.

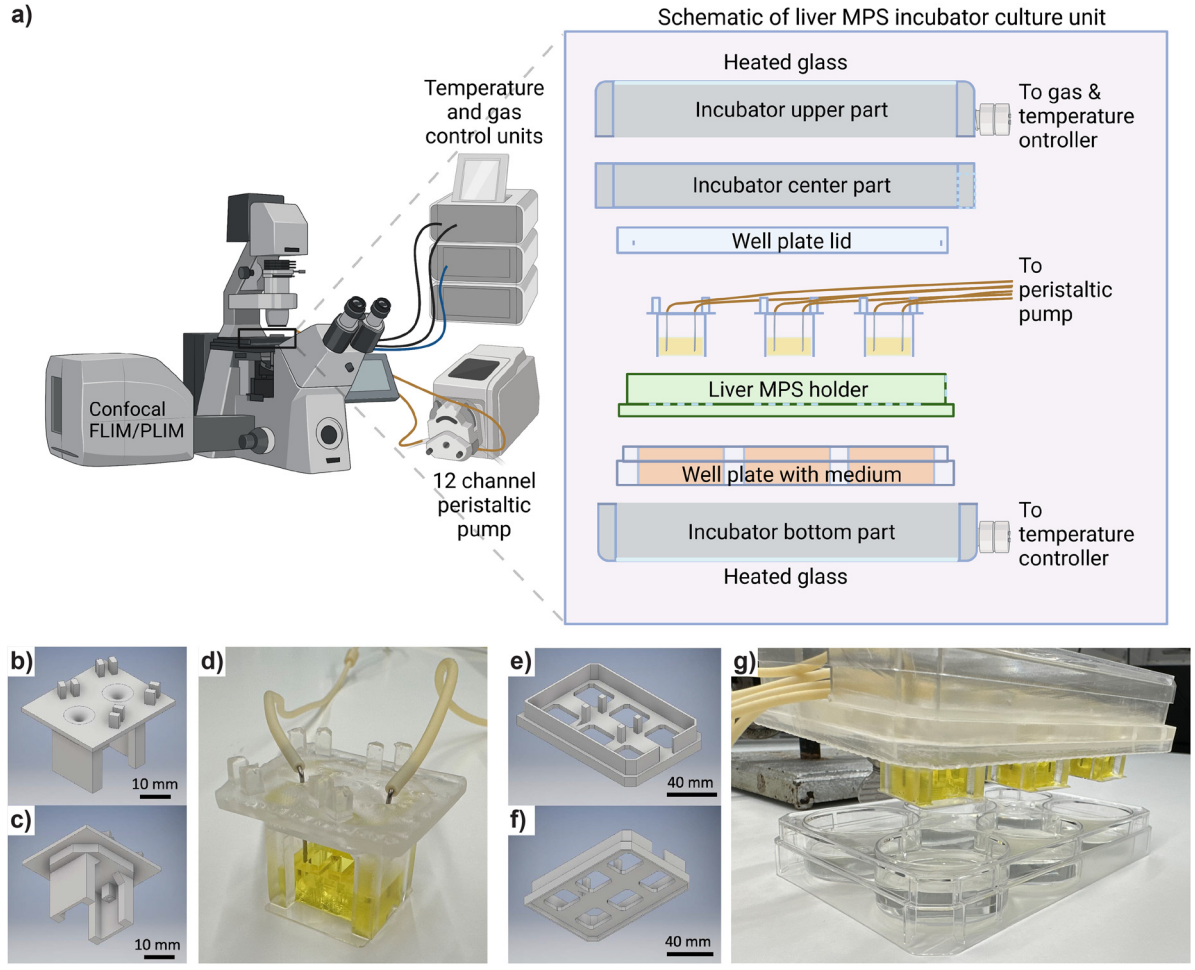

Fig. 2. Depiction of the experimental setup. (a) Schematic of liver MPS culture setup consisting of a confocal FLIM/PLIM microscope, peristaltic pump, gas controller, and a custom-built microscope-compatible incubator and temperature controller. The incubator has electrically heated, temperature controlled, aluminum side walls and electrically heated top and bottom glasses to minimize temperature gradients across all culture volumes and to avoid water condensation on the glass bottomthat compromises visual access. MPS scaffolds are cultured in small holders (b-d) in a standard 6-well plate with a 3D printed liver MPS holder having cut-outs for the small holders (e-g). Aseptic conditions during long-term culture are maintained using lids of holders and the well plate, and by supplying the assembled fully airtight incubator with a filtered gas mixture.

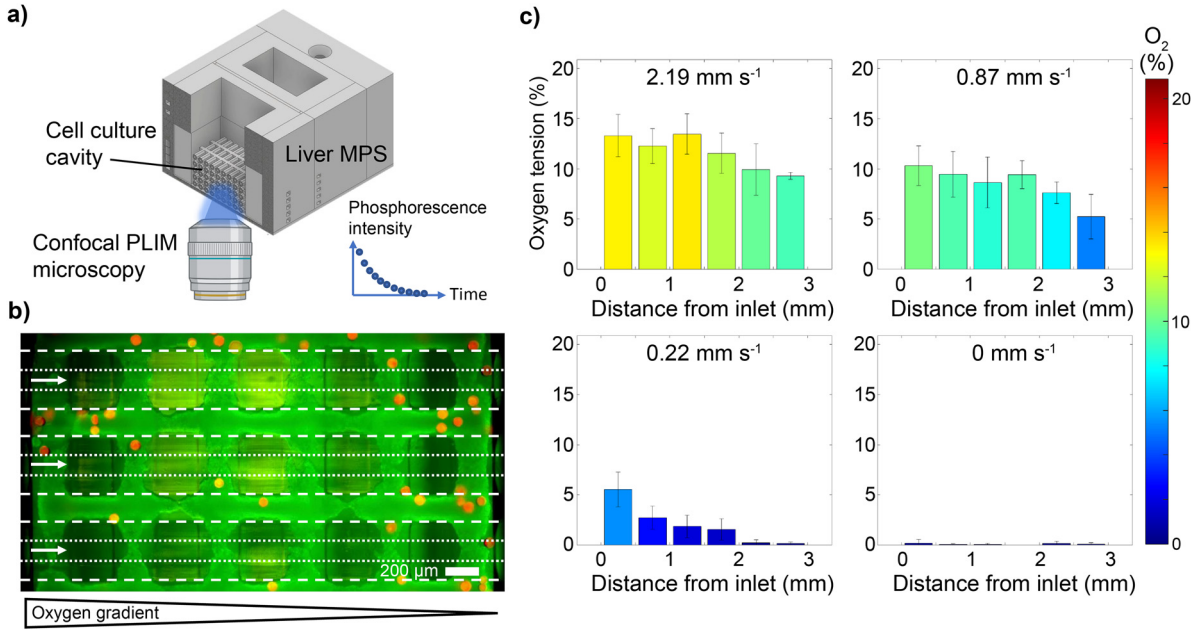

Fig. 3. Oxygen gradient assessment in liver MPS at different flow rates using phosphorescent lifetime-based 3D oxygen mapping method allows multipoint, spatially resolved oxygen mapping during perfusion culture. (a) Schematic of a 3D printed liver MPS, optically scanned during perfusion culture with a confocal phosphorescence lifetime imaging microscope. (b) Overlaid fluorescence (green) and phosphorescence (red) micrographs of oxygen sensor beads (orange) embedded in a hydrogel-free 3D culture of Hep G2 cells (green; live stain by calcein AM) in a liver MPS. The dotted and dashed lines illustrate the inside and outside, respectively, of the channel walls, and the arrows show the flow direction. The apparent orange color of the sensor beads in this combined color micrograph is due to the oxygen sensitive platinum species having both short-lived fluorescence emission (colored green) and long-lived phosphorescence emission (colored red). The apparent bead colors are only used to illustrate the bead locations in the cell volume and are unrelated to the local oxygen tension, which can only be extracted from analysis of the individual bead's phosphorescence decay lifetime. (c) Oxygen tension profile throughout a single cavity with a length of approximately 2.8 mm for the indicated average perfusion velocities (flow rates of 200 µL min^{-1}, 80 µL min^{-1}, 20 µL min^{-1}, and 0 µL min^{-1}, respectively). Imaging windows of approximately 2.8 mm × 2 mm are applied, and the readout from sensor beads is grouped by position in bins of 0.5 mm length (n = 5–14 in each bin). Error bars show the standard deviation.

3.3. 3D oxygen gradient measurements

Studies of oxygen gradients in the human liver most commonly report the oxygen tension in periportal ≈8% (60–65 mmHg) and perivenous ≈4% (30–35 mmHg) blood [26]. Tissue oxygen concentrations are more difficult to measure, with reported values of ≈3% (20–25 mmHg) using microelectrodes [27]. The intracellular *in vivo* oxygen gradient across the different zones has been estimated to range from ≈6% (45–50 mmHg) on the periportal side of the acinus to ≈2% (15–20 mmHg) on the perivenous side [11]. We tested whether such physiological oxygen gradients could be recreated in the liver MPS *in vitro*, when perfusing with normoxic medium (19% / 142 mmHg dissolved O_2 at 37 °C and 5% CO_2 [19]) at an optimized flow rate. To this end, we populated each liver MPS with 4 million hepatic Hep G2 cells that rapidly formed a continuous interconnected cell volume between the perfusion channels to a height of approximately 1.4 mm, as observed by confocal fluorescence microscopy (Fig. 3a,b). The oxygen consumption rate in human liver is reported to be 0.06 mL g^{-1} min^{-1} [28], corresponding to 4 × 10^{-8} mol cm^{-3} s^{-1} for an approximate liver mass density of 1 g cm^{-3}. Hep G2 cells were used in this part of the study, since their oxygen consumption rate per tissue volume, 4 × 10^{-17} mol $cell^{-1}$ s^{-1} [29] at an estimated compact cell density of 1.1 × 10^{9} cm^{-3} (cell volume of 850 µm^3 [30]) yielding 4 × 10^{-8} mol cm^{-3} s^{-1}, is a good approximation of human liver tissue. To map the oxygen gradient in the liver MPS, oxygen sensor beads were integrated during cell seeding (Fig. 3b). Subsequently, the beads were scanned with an inverted confocal phosphorescence lifetime microscope and analyzed with dedicated 3D oxygen mapping software [19]. Oxygen sensor beads located within the lower-most 0.5 mm of the culture volume were probed, with the probe depth limited by optical scattering through the dense aggregate of cells. All the discrete oxygen measurements were employed for making a binned distribution of the oxygen gradient along the flow direction. Four different flow velocities were tested to assess the relation between perfusion rate and oxygenation (Fig. 3c). In all four tested conditions, the maximum measured oxygen concentration was lower than in the perfusion medium due to the oxygen sensor beads being embedded in the dense oxygen-consuming cell volume. Flow velocity in microfluidic channels traversing the liver acinus model at 2.19 mm s^{-1} resulted in hyperoxygenation with an oxygen gradient in the cell compartment from ≈14% to ≈9%, while a flow speed of 0.22 mm s^{-1} resulted in an oxygen gradient from ≈5% to ≈0%, slightly below the estimated intracellular range *in vivo*. An intermediate flow speed of 0.87 mm s^{-1} generated an oxygen gradient from ≈10% to ≈4%, in close proximity of the measured gradient in liver acinus blood, and was consequently used in the rest of further experiments. Not surprisingly, cessation of flow resulted in rapid hypoxia within minutes with oxygenation levels close to 0% throughout the whole liver acinus construct. This is in agreement with our former results using a single layer of perfusion channels, where full anoxia in the cultured cell volume was observed within 10 min of stopping perfusion of medium [19].

3.4. The MPS supports long-term culture and improved differentiation of hiPSC-derived HLCs

Human iPSC-derived liver spheroids were seeded on day 7 of differentiation into liver MPS systems and cultured under perfusion culture for 54 days. Spheroids of 100–350 µm in diameter were seeded, which was enabled using an inter-channel spacing of 440 µm in the chip design. Simple pipetting of the spheroid suspension into the chip cavities resulted in a thick sediment of separate spheroids evenly distributed across the cavity area, in the

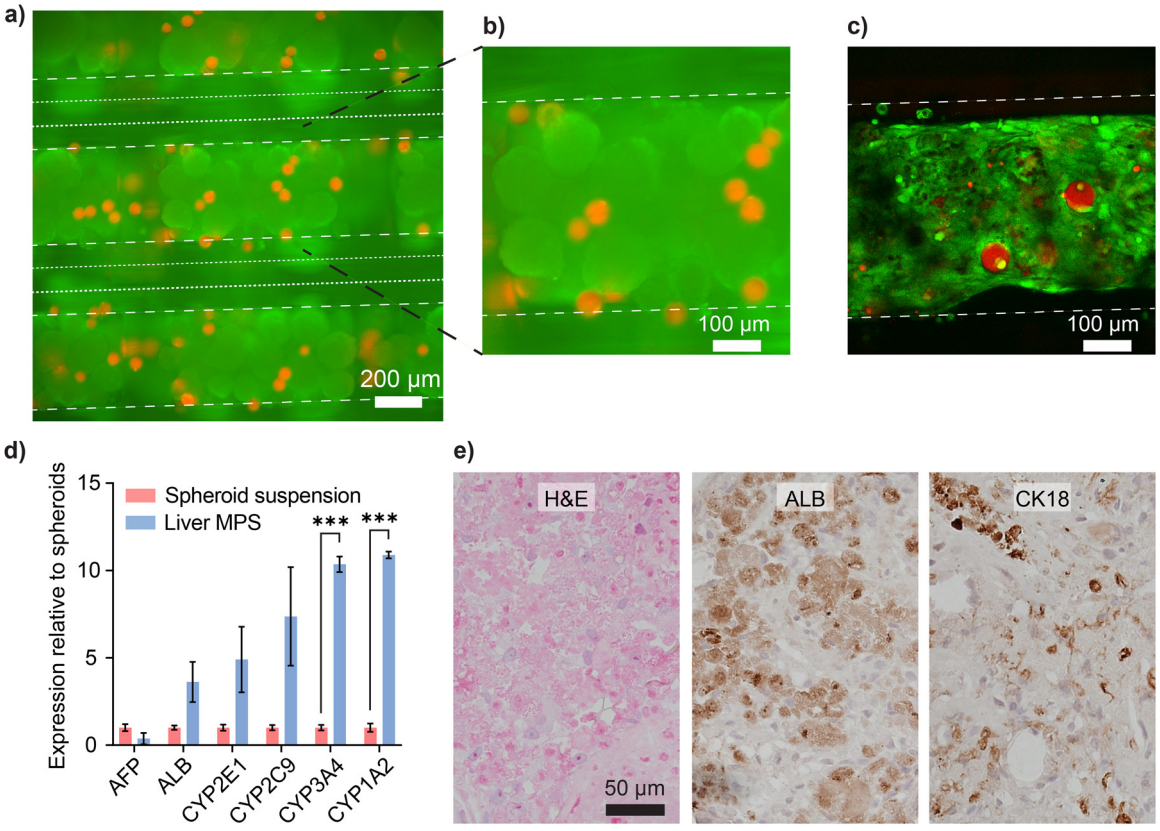

Fig. 4. iPSC-derived spheroid liver MPS culture. (a) Wide-field fluorescence micrograph of hiPSC-derived liver-like cells in spheroids on day 2 of culture with live cells (green) stained by perfusion of calcein-AM and CPOx Red oxygen sensor beads (red). (b) Zoom on the indicated area in (a). (c) Confocal fluorescence micrograph (maximum intensity projection) on day 40 with additional stain of dead cells (red) by perfused propidium iodide (large sensor beads appear red), acquired at a different chip area. (d) Expression of key genes of hiPSC-derived suspension spheroid culture and liver MPS culture compared by qPCR on day 60 after start of differentiation or day 54 of seeding in liver MPS (mean ± SEM, $n = 3$, data normalized to expression of spheroid cultures, *** $p < 0.001$). (e) Optical micrographs of sections of fixed and isolated tissues from liver MPS culture from day 60 of differentiation. Tissues stained with hematoxylin-eosin (H&E) and antibodies for albumin (ALB) and cytokeratin 18 (CK18).

absence or presence of suspended oxygen sensor beads (Fig. 4a-b). The development of the system was monitored by microscopy at regular intervals. An MPS culture stained for live cell marker calcein AM and dead cell marker propidium iodide on day 40 of culture showed clear fusion of spheroids into dense tissues and with little visible cell death (Fig. 4c). Expression profiling of liver markers obtained from tissues cultured for 54 days showed increased differentiation in the MPS compared to spheroid suspension culture, as indicated by strongly elevated expression of hepatic markers, CYP enzymes and albumin, and with decreased expression of the progenitor cell marker *AFP* (Fig. 4d). Furthermore, immunohistochemical analyses of hiPSC-derived MPS tissue sections confirmed the formation of a dense continuous tissue with clear protein expression of the hepatocyte markers ALB and CK18 [31] (Fig. 4e).

3.5. The primary human hepatocyte liver MPS allows the long-term maintenance of physiologically relevant phenotypes and functions

Next, we assessed the ability of the device for long-term culture of primary human liver cells. While cells remained round and clearly visible as individual units after seeding, the seeded cells compacted and had merged into an interconnected tissue after five days of perfusion culture (Fig. 5a). In contrast, when cultured without perfusion through the synthetic vasculature, cells remained round and did not aggregate due to very limited or absent metabolic activity in their environment depleted of oxygen and nutrients (Figure S3). Morphologically, the perfused tissue remained intact and limited remodeling was visible after tissue formation throughout the culture period.

To profile the molecular phenotypes of the MPS liver constructs, we evaluated expression of secreted hepatic factors (*ALB*), drug metabolizing enzymes (*CYP2E1, CYP3A4, CYP2C8, CYP2D6* and *CYP4F12*), and factors involved in fatty acid and carbohydrate metabolism (*FASN, SREBF1,* and *PCK1*). Notably, expression levels were orders of magnitude higher than in 2D culture and similar or even higher than in 3D spheroids (Fig. 5b; Figure S4). Particularly, the perivenous zonation markers *CYP3A4* and *CYP2E1* were significantly increased in the MPS, indicating molecular zonation without a deterioration in overall phenotypes. These observations were supported by biochemical methods, which showed that secretion of albumin as a marker of hepatocyte cell health and function remained constant throughout long-term culture (Fig. 5c). The apparent reduction at day 14 is due to a shorter collection time in the experimental setup for this data point, and expression analysis of *ALB* in Fig. 5b did also show equivalent levels in 3D spheroids and MPS cultures. Furthermore, we corroborated hepatocyte function by evaluating *CYP3A4* induction using the *bona fide* nuclear hormone receptor ligand rifampicin (Fig. 5d). After 72 h of rifampicin exposure, the perfused liver MPS system showed induction of *CYP3A4* expression similar to spheroids, the gold standard for preclinical CYP induction measurements [32], suggesting that nuclear hormone receptor signaling and cellular xenobiotic sensing remains intact. To further validate that metabolic activity of PHH was maintained and responsive to exogeneous induction, we evaluated the metabolic activity of *CYP3A4* and *CYP2C8* in the liver MPS. Specifically, we exposed the device to the probe

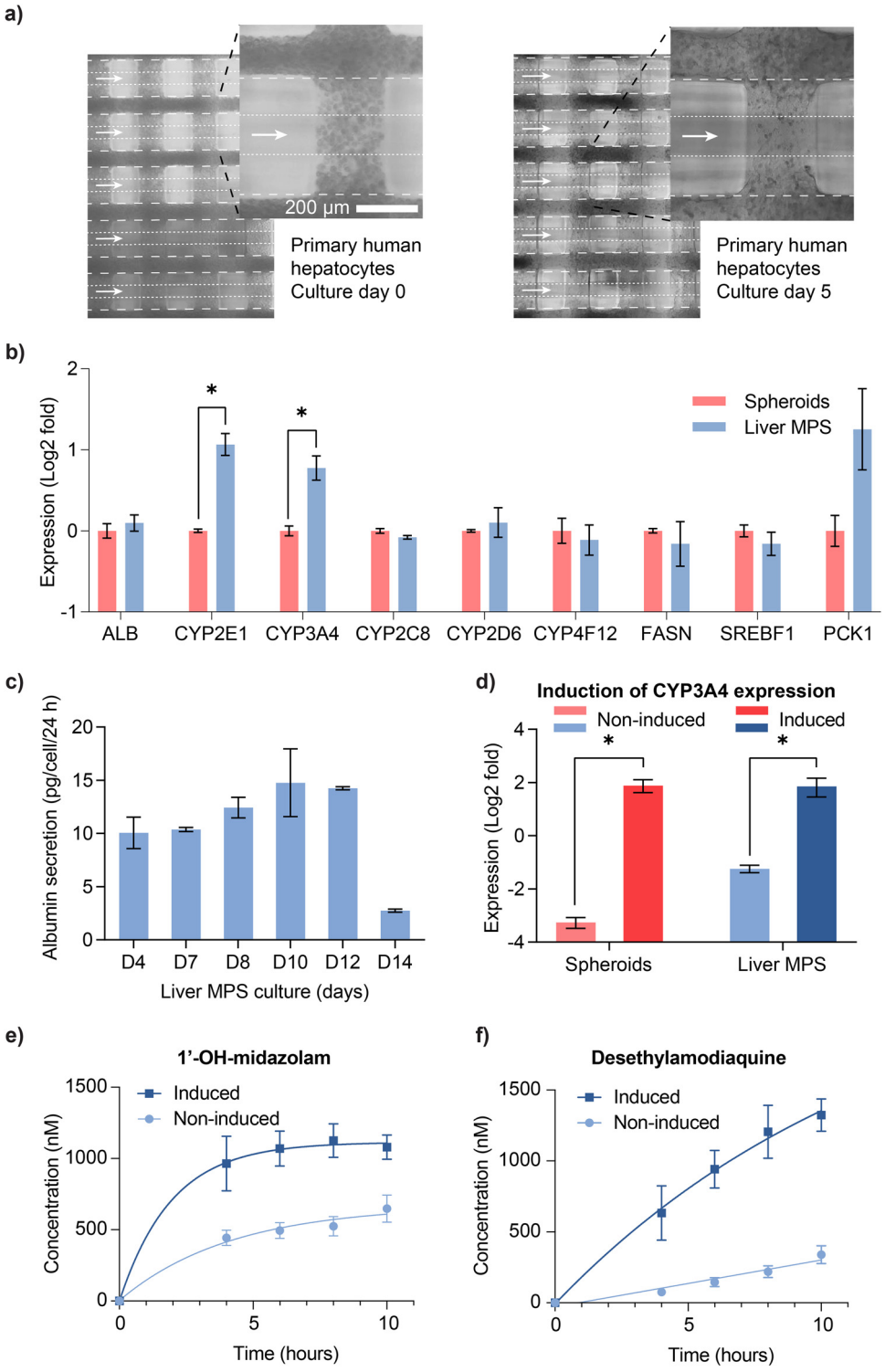

Fig. 5. Tissue formation and functional assessment of primary liver MPS. (a) Phase contrast micrographs of cultures shortly after seeding (day 0) and after tissue formation (day 5) at a perfusion rate of 120 µL min^{-1}. (b) Expression analysis by qPCR on day 14 of spheroid cultures and liver MPS cultures (mean ± SEM, $n = 3$, data normalized to expression of spheroid cultures, * $p < 0.05$). (c) Albumin secretion over the course of 14 days ($n = 3$). (d) Induction of CYP3A4 expression by treatment of induced samples with 10 µM rifampicin for 48 h prior to assay run on day 14, data normalized to expression at day 0 ($n = 3$). (e-f) Metabolic assay data from control and induced liver MPS, where induced samples are treated with 10 µM rifampicin for 72 h prior to assay run ($n = 3$). For comparison of control and induced liver MPS, induced samples were adjusted with a factor 1.13 to correct for the difference in seeded cell numbers.

substrates midazolam (*CYP3A4*) and amodiaquine (*CYP2C8*) and evaluated their metabolic conversion to 1′-OH-midazolam (Fig. 5e) and *N*-desethylamodiaquine (Fig. 5f) by mass spectrometry in control and induced liver MPS. The metabolic analysis of control samples on day 14 of culture revealed 443±55 nM of 1′-OH-midazolam and 76±16 nM of *N*-desethylamodiaquine in 4 h, corresponding to metabolite formation rates of 8.3 pmol/min/10^6 cells and 1.4 pmol/min/10^6 cells, respectively. Induction of PXR using rifampicin for 72 h prior to the start of the measurement increased total metabolite formation to 964±192 nM and 633±192 nM for

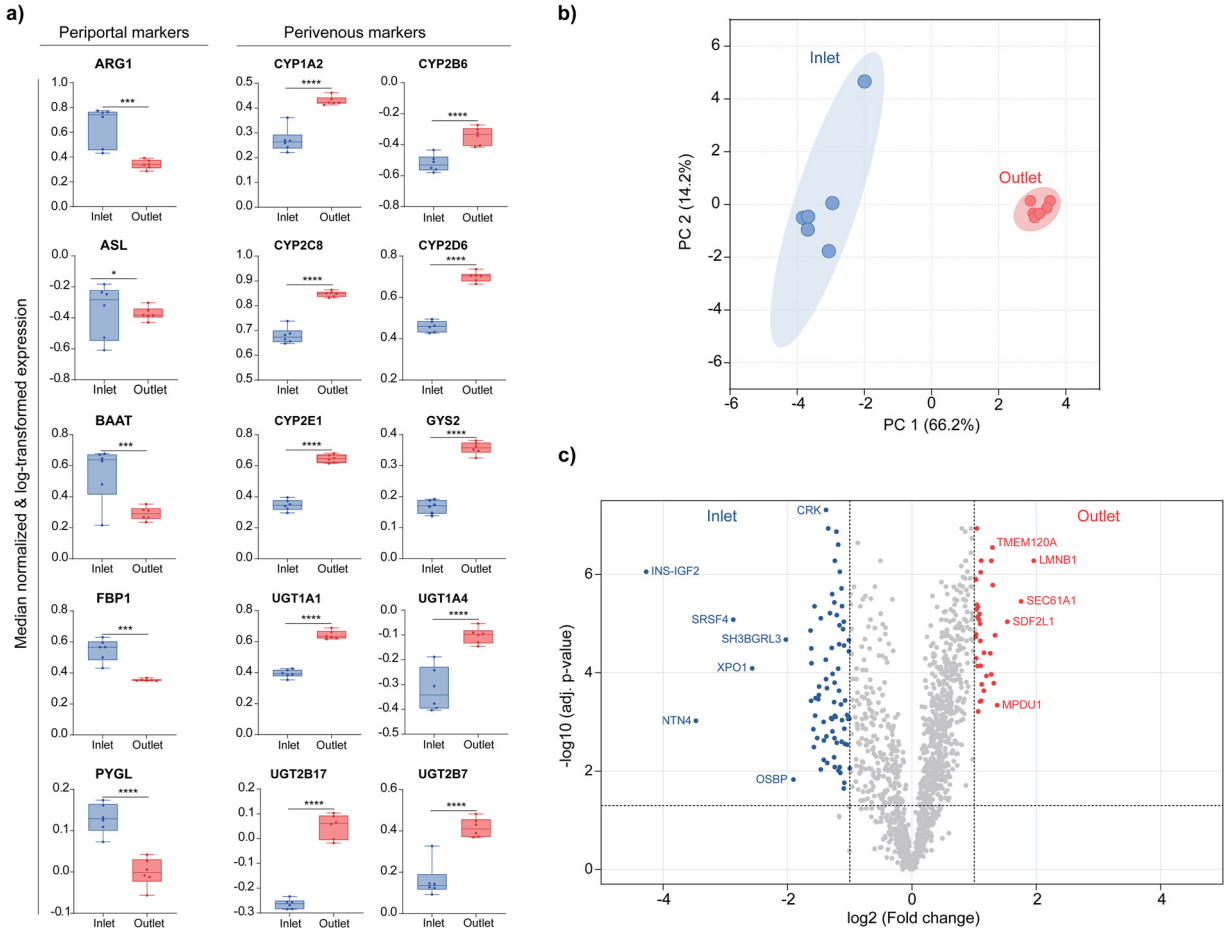

Fig. 6. Proteomic analysis of hepatic zonation in the liver MPS using a non-targeted mass spectrometry-based approach. (a) Box plots showing the median-normalized and log-transformed abundance for differentially expressed periportal and perivenous proteins on the inlet (left) and outlet (right) of the liver MPS ($n = 6$; * $p < 0.05$, ** $p < 0.01$, *** $p < 0.001$, **** $p < 0.0001$). (b) Principal component analysis (PCA) of proteomics data from the inlet and outlet side of the liver MPS. The PCA plot represents biological replicates with 1398 quantified proteins, which indicates clear profile differences between the samples from inlets and outlets ($n = 6$) grouped by color. (c) Volcano plot of zonal differences (log2 of the ratio of abundances of each protein at the outlet side and inlet side) of MPS samples ($n = 6$).

1′-OH-midazolam and *N*-desethylamodiaquine, respectively, confirming the ability of the system to capture drug-drug interactions via an intact nuclear hormone receptor signaling axis.

3.6. Non-targeted proteomics reveals comprehensive molecular zonation into periportal and perivenous hepatocytes in the liver MPS

To evaluate whether the microperfused liver MPS allowed for a recapitulation of hepatic zonation, we performed a comprehensive proteomics investigation. To this end, we first compared expression of known zonation markers [33–35] in the inlet and outlet sides of the device. Close to the inlet, where oxygen concentrations are highest, we observed increased levels of the periportal marker proteins ARG1, BAAT, PYGL, FBP1 and ASL (Fig. 6a). In contrast, expression of perivenous markers was significantly elevated close to the outlet where oxygenation is lower. When analyzing the proteomic signatures comprehensively, we found that hepatocytes on the inlet and outlet sides of the microperfused liver MPS could be clearly separated (Fig. 6b). Among the top proteins with the highest differences in zonal expression were the signal transducer CKL and the metabolic regulator INS-IGF2, which were upregulated on the inlet side, as well as structural components (LMNB1) and chaperones (SDF2L1) on the outlet side (Fig. 6c). Notably, pathway analysis of the differentially expressed proteins revealed that, among other functions, biosynthesis of amino acids and gluconeogenesis were increased at the inlet region, whereas drug metabolism, amino acid degradation, steroid hormone biosynthesis and fatty acid metabolism were upregulated close to the outlet (Table 1). Importantly, in contrast to previous studies [12], zonation in this device is naturally generated by high cell densities and the corresponding oxygen and nutrient utilization along the flow path. These results thus demonstrate that our *in vitro* 3D liver model can provide a reliable tool for studying spatial phenotypic variations of primary human liver cells in a controlled microenvironment.

3.7. The primary human hepatocyte liver MPS recapitulates functional zonation

To test whether hepatic zonation at the level of gene expression also translated into functional differences, we tested if the liver MPS could recapitulate zone-specific hepatotoxicity. To this end, we exposed the primary human liver MPS to different concentrations of acetaminophen (APAP), which is mainly metabolized by the perivenous CYP enzymes CYP2E1 and CYP3A4 into the reactive and hepatotoxic metabolite *N*-acetyl-*p*-benzoquinoneimine (NAPQI). We evaluated spatial toxicity patterns using live/dead staining and quantified the resulting signals as a function of axial position. Plasma concentrations of APAP above 2 mM (300 mg L^{-1}) in humans are known to cause partial liver damage [36]. At low concentrations (1–3 mM APAP) we observed no measurable cell death, whereas complete cell death was observed at a very high concentration of 50 mM (Fig. 7). Importantly, however, at intermediate APAP concentrations of 5 mM, cytotoxicity was clearly graded. Cell death was overall low on the highly

Table 1
Selected differentially regulated pathways in the inlet (periportal) and outlet (perivenous) side of the liver MPS. FDR = false discovery rate.

Zone	Pathway	Size	Enrichment ratio	P Value	FDR
Inlet	Biosynthesis of amino acids	75	8.44	3.4×10^{-13}	5.5×10^{-11}
	Fructose and mannose metabolism	33	8.08	4.2×10^{-6}	1.9×10^{-4}
	Pentose phosphate pathway	30	7.78	2.2×10^{-5}	7.3×10^{-4}
	Cysteine and methionine metabolism	47	6.38	8.4×10^{-6}	3.4×10^{-4}
	Gluconeogenesis	68	6.37	8.1×10^{-8}	5.3×10^{-6}
Outlet	Valine. leucine and isoleucine degradation	48	8.93	$<2.2 \times 10^{-16}$	$<2.2 \times 10^{-16}$
	Drug metabolism	72	6.99	1.1×10^{-16}	3.3×10^{-15}
	Retinol metabolism	67	6.12	1.8×10^{-12}	4.9×10^{-11}
	Fatty acid metabolism	48	5.82	1.4×10^{-8}	2.3×10^{-7}
	Steroid hormone biosynthesis	60	5.28	8.2×10^{-9}	1.4×10^{-7}
	Protein processing in endoplasmic reticulum	165	4.74	$<2.2 \times 10^{-16}$	$<2.2 \times 10^{-16}$

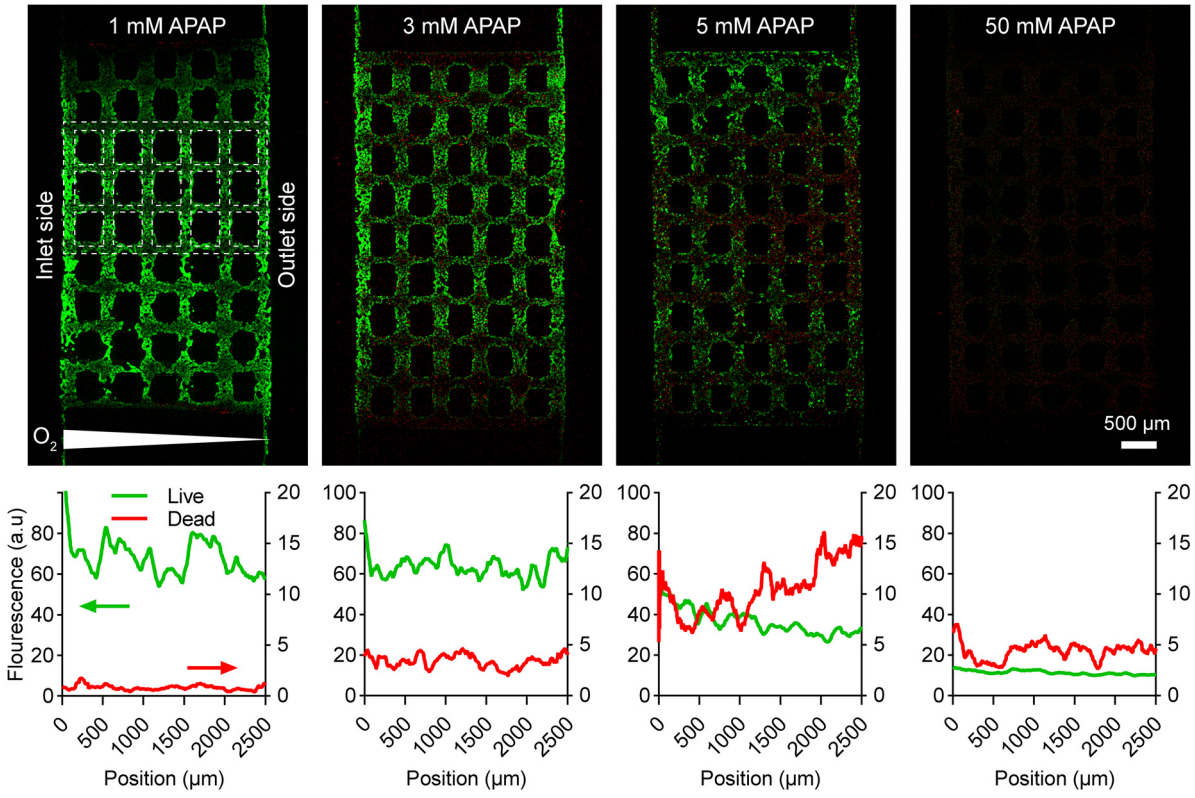

Fig. 7. Spatially resolved drug toxicity in PHH liver MPS. Individual liver MPS's were cultured for 8 days without drug followed by 7 days of culture with acetaminophen (APAP) at the specified concentrations (1 mM, 3 mM, 5 mM, 50 mM). Representative fluorescence micrographs (upper row; maximum intensity projection) show cultures stained for enzymatically active (green; calcein AM) and non-viable (red; propidium iodide) cells on day 15. The position dependent viability of each culture (lower row) is assessed by quantifying the average green (left axis) and red (right axis) fluorescence intensity (arbitrary units) from inlet side to outlet side, vertically averaged within the region between dashed areas. Similar patterns in live and dead cell distributions were observed in 3 independent experiments using a concentration of 5 mM APAP. The reduced intensity of the red signal (non-viable cells) at the highest APAP concentration is likely due to prior disintegration of most cells, leaving few polynucleotides to stain. All micrographs were acquired using the same microscopy settings.

oxygenated periportal side and then continuously increased towards the slightly oxygenated perivenous side. Notably, these patterns of toxicity are in agreement with the increased expression of the perivenous markers CYP2E1 and CYP3A4 in the liver MPS, which drive APAP hepatotoxicity, and recapitulate *in vivo* APAP toxicity profiles [37]. Thus, these results suggest that the physiological oxygen gradient in the liver MPS entails the establishment of zonal identities at the molecular level, which further translates into differences at the functional level that cannot be captured in conventional 3D static culture.

4. Discussion

Emulating human liver functions *in vitro* constitutes an important milestone for understanding liver biology in health and disease, as well as for the preclinical development of new chemical entities. Over the past decade, it has become increasingly clear that conventional *in vitro* methods, such as 2D monolayer cultures of human hepatocytes, rapidly deteriorate, which limits their utility to short-term applications. While a multitude of hepatic 3D culture methods, such as liver spheroids and micropatterned co-cultures have drastically extended the functional *in vitro* culture time of PHH [38], important limitations remain. These include the absence of functional zonation as well as the relatively low cell density. Here, we attempted to ameliorate these issues by implementing an MPS with parallel microperfusion channel arrays 3D printed in a fully automated process. The results clearly support that the device can sustain the functional long-term culture of engineered human liver tissue comprised of both primary human hepatocytes and human induced pluripotent-derived liver-like cells at unprecedented

in vivo-like cell densities of >100 million cells mL^{-1}. Oxygen utilization in these mesoscale tissue constructs drove the formation of a physiologically relevant oxygen gradient, which propagated into functional specification. Moreover, direct contact with perfusion medium is avoided in the diffusion-open synthetic vasculature chips, which results in similar protection of hepatocytes to shear forces as *in vivo*. The resulting tissue formation, cell survival and maintenance of phenotype, presented in this work, indicate that the created microenvironments are suitable for high density 3D liver-live cultures without the need for embedding hydrogels.

The hiPSC-based liver-like spheroid based MPS cultures enabled the formation of dense, interconnected 3D tissues and exhibited high viability in long-term cultures (2 months), assessed by live/dead stained liver MPS. Expression profiling showed a significant increase in liver typical markers in the liver MPS compared to spheroid suspension cultures at day 60 of differentiation. Thus, our liver MPS seems more suitable than 3D suspension cultures to improve maturation of hiPSC-derived liver tissues, hypothesized to stem from the absence of shear stress, improved cell-cell communication, and higher local concentration of tissue excreted signaling compounds. The confirmation of the presence of liver typical proteins such as albumin in histological analysis of the liver tissues further supports this and the presence of cytokeratin 18, expressed on hepatocyte plasma membrane surface, confirms the presence of hepatocyte-like cells.

MPS cultures from seeded PHH also fused into dense interconnected 3D tissues after 3–5 days of culture. Seeded tissue densities can be estimated from the volume of 1 million primary human hepatocytes with an average cellular volume of 2.3×10^3 μm^3 [39] resulting in 2.3 µL total cell volume. This corresponds to an upper limit on the cell density of 4.3×10^8 cells mL^{-1} located within the MPS acinus model volume of 20 µL (excluding the synthetic vasculature channels). The looser initially formed tissue is observed to contract further during the first 5 days of culture and likely forms more dense tissues between the vasculature channels while forming small voids around it. This was contrasted by the failure of cells to fuse into dense, connected tissues in control liver MPS cultures with disabled perfusion leading to tissue anoxia. This highlighted the necessity of dense, perfused synthetic vasculature to establish suitable microenvironments that support tissue formation.

The primary hepatocyte MPS results show that the system not only promotes primary hepatocyte survival but also supports high maintenance of liver-typic expression profiles, which vastly improved over 2D cultures and also over 3D spheroid cultures. A mature liver phenotype could be maintained over the course of 14 days as indicated by albumin secretion levels significantly higher than those in 2D cultures. The metabolite formation rates for 1′-OH-midazolam and *N*-desethylamodiaquine observed in this study are at comparable levels to those previously observed in 3D spheroids [23].

The dose dependent APAP toxicity assay with clearly decreasing cell viability at 5 mM indicates high sensitivity to toxic drug compound screening at physiologically relevant concentrations. The dose responses seen in this study are similar to doses previously used in 3D primary hepatocyte spheroids [40] and close to *in vivo* levels for APAP overdosing resulting in drug induced liver injury or failure [41]. Importantly, a zonated toxicity with intermediate cell viability on the higher oxygenated periportal side and reduced viability on the lower oxygenated perivenous side of the liver acinus MPS was apparent from quantification of the fluorescent viability probe at 5 mM APAP. This result is in excellent agreement with prior zone-dependent *in vitro* APAP dose responses of primary rat hepatocytes [42].

The MPS established here can provide a useful platform for applications that require physiological cell densities. Specifically, the system opens the possibility to identify mechanistic biomarkers of liver injury that are often of low abundance slightly abundant. These include molecular signatures as markers for hepatic fibrosis [43,44], metabolomic biomarkers for drug-induced liver injury [45], as well as secreted extracellular vesicles as markers for alcoholic liver disease [46] and the formation of pre-metastatic liver niches [47]. Furthermore, high cell densities in the MPS enable its use for the analysis of low-clearance drugs, which cannot be measured in conventional spheroid cultures [48].

5. Conclusion

We developed and characterized a liver MPS with integrated perfused synthetic vasculature that enabled the recapitulation of liver acinus models with an *in vivo*-like oxygen gradient. Freeform 3D printing of diffusion-open synthetic vasculature chips allowed for massive parallel microperfusion in three independent culture cavities per chip, enabling stable, long-term perfusion cultures with live imaging capabilities. hiPSC-based liver MPS allowed the use of hiPSC-derived hepatocyte-like spheroids in long-term cultures (up to 2 months) with improved maturation compared to spheroid suspension culture. Primary human hepatocyte-based liver MPS showed formation of dense 3D tissues with high viability and preserved liver function over the course of 14 days compared to 2D culture. Dose-dependent APAP toxicity assays revealed zonated toxicity patterns, with higher toxicity in the perivenous side of the acinus compared to the periportal. In future work, further benchmarking with other cell sources, both iPSC-derived as well as primary human and animal cells, screening of larger drug libraries, further confirmation of zonation and the establishment of disease models would be of high interest. We conclude that the developed liver MPS is suitable for the organotypic long-term culture of human liver cells and replicates *in vivo*-like continuous oxygen gradients in connected mesoscale liver tissue.

Declaration of Competing Interest

The authors declare the following financial interests/personal relationships which may be considered as potential competing interests: Lena C. Preiss reports financial support was provided by Merck KGaA. Volker M. Lauschke reports a relationship with HepaPredict AB and PersoMedix AB that includes: employment and equity or stocks. Voler M. Lauschke reports a relationship with Enginzyme AB that includes: consultancy.

Acknowledgements

The work was funded by Independent Research Fund Denmark (grant number 7017–00366B and 2035-00186B), the Novo Nordisk Foundation (grant number NNF16OC0022166), the Technical University of Denmark, Department of Health Technology, the Swedish Research Council (grant agreement numbers: 2016–01153, 2016–01154 and 2019–01837), by the EU/EFPIA/OICR/McGill/KTH/Diamond Innovative Medicines Initiative 2 Joint Undertaking (EUbOPEN grant number 875510) and by the Robert Bosch Foundation, Stuttgart, Germany. This work was partly supported by the Research Council of Norway through its Centres of Excellence funding scheme (project number 262613 to GS), and FRIPRO grants (project number 247624 to GS).

Supplementary materials

Supplementary material associated with this article can be found, in the online version, at doi:10.1016/j.actbio.2023.09.022.

References

[1] S. Youhanna, A.M. Kemas, L. Preiss, Y. Zhou, J.X. Shen, S.D. Cakal, F.S. Paqualini, S.K. Goparaju, R.Z. Shafagh, J.U. Lind, C.M. Sellgren, V.M. Lauschke, Organotypic and microphysiological human tissue models for drug discovery and development—current state-of-the-art and future perspectives, Pharmacol. Rev. 74 (2022) 141–206, doi:10.1124/pharmrev.120.000238.

[2] V.M. Lauschke, S.U. Vorrink, S.M.L. Moro, F. Rezayee, Å. Nordling, D.F.G. Hendriks, C.C. Bell, R. Sison-Young, B.K. Park, C.E. Goldring, E. Ellis, I. Johansson, S. Mkrtchian, T.B. Andersson, M. Ingelman-Sundberg, Massive rearrangements of cellular MicroRNA signatures are key drivers of hepatocyte dedifferentiation, Hepatology 64 (2016) 1743–1756, doi:10.1002/hep.28780.

[3] J.A. Heslop, C. Rowe, J. Walsh, R. Sison-Young, R. Jenkins, L. Kamalian, R. Kia, D. Hay, R.P. Jones, H.Z. Malik, S. Fenwick, A.E. Chadwick, J. Mills, N.R. Kitteringham, C.E.P. Goldring, B.Kevin Park, Mechanistic evaluation of primary human hepatocyte culture using global proteomic analysis reveals a selective dedifferentiation profile, Arch. Toxicol. 91 (2017) 439–452, doi:10.1007/s00204-016-1694-y.

[4] V.M. Lauschke, D.F.G. Hendriks, C.C. Bell, T.B. Andersson, M. Ingelman-Sundberg, Novel 3D culture systems for studies of human liver function and assessments of the hepatotoxicity of drugs and drug candidates, Chem. Res. Toxicol. 29 (2016) 1936–1955, doi:10.1021/acs.chemrestox.6b00150.

[5] C. Lin, S.R. Khetani, Advances in engineered liver models for investigating drug-induced liver injury, Biomed Res. Int 2016 (2016) 1–20, doi:10.1155/2016/1829148.

[6] V.M. Lauschke, R.Z. Shafagh, D.F.G. Hendriks, M. Ingelman-Sundberg, 3D primary hepatocyte culture systems for analyses of liver diseases, drug metabolism, and toxicity: emerging culture paradigms and applications, Biotechnol. J. 14 (2019) 1–12, doi:10.1002/biot.201800347.

[7] X. Zhang, T. Jiang, D. Chen, Q. Wang, L.W. Zhang, Three-dimensional liver models: state of the art and their application for hepatotoxicity evaluation, Crit. Rev. Toxicol. 50 (2020) 279–309, doi:10.1080/10408444.2020.1756219.

[8] N.S. Bhise, V. Manoharan, S. Massa, A. Tamayol, M. Ghaderi, M. Miscuglio, Q. Lang, Y.S. Zhang, S.R. Shin, G. Calzone, N. Annabi, T.D. Shupe, C.E. Bishop, A. Atala, M.R. Dokmeci, A. Khademhosseini, A liver-on-a-chip platform with bioprinted hepatic spheroids, Biofabrication 8 (2016) 14101, doi:10.1088/1758-5090/8/1/014101.

[9] H. Lee, S. Chae, J.Y. Kim, W. Han, J. Kim, Y. Choi, D.W. Cho, Cell-printed 3D liver-on-a-chip possessing a liver microenvironment and biliary system, Biofabrication 11 (2019) 25001, doi:10.1088/1758-5090/aaf9fa.

[10] M. Ingelman-Sundberg, V.M. Lauschke, 3D human liver spheroids for translational pharmacology and toxicology, Basic Clin. Pharmacol. Toxicol. 130 (2022) 5–15, doi:10.1111/bcpt.13587.

[11] T. Kietzmann, Metabolic zonation of the liver: the oxygen gradient revisited, Redox Biol. 11 (2017) 622–630, doi:10.1016/j.redox.2017.01.012.

[12] L. Tomlinson, L. Hyndman, J.W. Firman, R. Bentley, J.A. Kyffin, S.D. Webb, S. McGinty, P. Sharma, *In vitro* liver zonation of primary rat hepatocytes, Front. Bioeng. Biotechnol. 7 (2019) 1–8, doi:10.3389/fbioe.2019.00017.

[13] B. Scheidecker, M. Shinohara, M. Sugimoto, M. Danoy, M. Nishikawa, Y. Sakai, Induction of *in vitro* metabolic zonation in primary hepatocytes requires both near-physiological oxygen concentration and flux, Front. Bioeng. Biotechnol. 8 (2020) 1–17, doi:10.3389/fbioe.2020.00524.

[14] F. Tonon, G.G. Giobbe, A. Zambon, C. Luni, O. Gagliano, A. Floreani, G. Grassi, N. Elvassore, *In vitro* metabolic zonation through oxygen gradient on a chip, Sci. Rep. 9 (2019) 13557, doi:10.1038/s41598-019-49412-6.

[15] F.T. Lee-Montiel, S.M. George, A.H. Gough, A.D. Sharma, J. Wu, R. DeBiasio, L.A. Vernetti, D.L. Taylor, Control of oxygen tension recapitulates zone-specific functions in human liver microphysiology systems, Exp. Biol. Med. 242 (2017) 1617–1632, doi:10.1177/1535370217703978.

[16] P. Sphabmixay, M.S.B. Raredon, A.J.S. Wang, H. Lee, P.T. Hammond, N.X. Fang, L.G. Griffith, High resolution stereolithography fabrication of perfusable scaffolds to enable long-term meso-scale hepatic culture for disease modeling, Biofabrication 13 (2021) 045024, doi:10.1088/1758-5090/ac23aa.

[17] Y. Yajima, C.N. Lee, M. Yamada, R. Utoh, M. Seki, Development of a perfusable 3D liver cell cultivation system via bundling-up assembly of cell-laden microfibers, J. Biosci. Bioeng. 126 (2018) 111–118, doi:10.1016/j.jbiosc.2018.01.022.

[18] R. Zhang, N.B. Larsen, Stereolithographic hydrogel printing of 3D culture chips with biofunctionalized complex 3D perfusion networks, Lab Chip 17 (2017) 4273–4282, doi:10.1039/C7LC00926G.

[19] M.F. Wesseler, M. Nørbæk Johansen, A. Kiziltay, K. Mortensen, N.B. Larsen, Optical 4D oxygen mapping of microperfused tissue models with tunable in vivo-like 3D oxygen microenvironments, Lab Chip 22 (2022) 4167–4179, doi:10.1039/D2LC00063F.

[20] Colibri Photonics, (n.d.). http://www.colibri-photonics.com/index.php/research (accessed July 29, 2023).

[21] S.P. Harrison, R. Siller, Y. Tanaka, Y. Xiang, B. Patterson, H. Kempf, E. Melum, K.S. Asrud, M.E. Chollet, E. Andersen, P.M. Sandset, S. Baumgarten, F. Bonanini, D. Kurek, S. Mathapati, R. Almaas, K. Sharma, S.R. Wilson, F.S. Skottvoll, I.C. Boger, I.L. Bogen, T.A. Nyman, J.J. Wu, A. Bezrouk, D. Cizkova, J. Mokry, R. Zweigerdt, I.-H. Park, G.J. Sullivan, Scalable production of tissue-like vascularised liver organoids from human PSCs, Exp. Mol. Med. (2023), doi:10.1038/s12276-023-01074-1.

[22] C.C. Bell, D.F.G. Hendriks, S.M.L. Moro, E. Ellis, J. Walsh, A. Renblom, L. Fredriksson Puigvert, A.C.A. Dankers, F. Jacobs, J. Snoeys, R.L. Sison-Young, R.E. Jenkins, Å. Nordling, S. Mkrtchian, B.K. Park, N.R. Kitteringham, C.E.P. Goldring, V.M. Lauschke, M. Ingelman-Sundberg, Characterization of primary human hepatocyte spheroids as a model system for drug-induced liver injury, liver function and disease, Sci. Rep. 6 (2016) 1–13, doi:10.1038/srep25187.

[23] S.U. Vorrink, S. Ullah, S. Schmidt, J. Nandania, V. Velagapudi, O. Beck, M. Ingelman-Sundberg, V.M. Lauschke, Endogenous and xenobiotic metabolic stability of primary human hepatocytes in long-term 3D spheroid cultures revealed by a combination of targeted and untargeted metabolomics, FASEB J 31 (2017) 2696–2708, doi:10.1096/fj.201601375R.

[24] J. Schindelin, I. Arganda-Carreras, E. Frise, V. Kaynig, M. Longair, T. Pietzsch, S. Preibisch, C. Rueden, S. Saalfeld, B. Schmid, J.Y. Tinevez, D.J. White, V. Hartenstein, K. Eliceiri, P. Tomancak, A. Cardona, Fiji: an open-source platform for biological-image analysis, Nat. Methods. 9 (2012) 676–682, doi:10.1038/nmeth.2019.

[25] Y. Liao, J. Wang, E.J. Jaehnig, Z. Shi, B. Zhang, WebGestalt 2019: gene set analysis toolkit with revamped UIs and APIs, Nucleic Acids Res 47 (2019) W199–W205, doi:10.1093/nar/gkz401.

[26] K. Jungermann, T. Kietzmann, Oxygen: modulator of metabolic zonation and disease of the liver, Hepatology 31 (2000) 255–260, doi:10.1002/hep.510310201.

[27] M. Kessler, Oxygen supply to tissue in normoxia and in oxygen deficiency, Microvasc. Res. 8 (1974) 283–290, doi:10.1016/S0026-2862(74)80004-X.

[28] J. Lutz, H. Henrich, E. Bauereisen, Oxygen supply and uptake in the liver and the intestine, Pflügers Arch, Eur. J. Physiol. 360 (1975) 7–15, doi:10.1007/BF00584322.

[29] F. Weise, U. Fernekorn, J. Hampl, M. Klett, A. Schober, Analysis and comparison of oxygen consumption of HepG2 cells in a monolayer and three-dimensional high density cell culture by use of a matrigrid®, Biotechnol. Bioeng. 110 (2013) 2504–2512, doi:10.1002/bit.24912.

[30] J.R. Wiśniewski, A. Vildhede, A. Norén, P. Artursson, In-depth quantitative analysis and comparison of the human hepatocyte and hepatoma cell line HepG2 proteomes, J. Proteomics. 136 (2016) 234–247, doi:10.1016/j.jprot.2016.01.016.

[31] G. Kania, P. Blyszczuk, A. Jochheim, M. Ott, A.M. Wobus, Generation of glycogen- and albumin-producing hepatocyte-like cells from embryonic stem cells, Biol. Chem. 385 (2004) 943–953, doi:10.1515/BC.2004.123.

[32] D.F.G. Hendriks, S.U. Vorrink, T. Smutny, S.C. Sim, Å. Nordling, S. Ullah, M. Kumondai, B.C. Jones, I. Johansson, T.B. Andersson, V.M. Lauschke, M. Ingelman-Sundberg, Clinically relevant cytochrome P450 3A4 induction mechanisms and drug screening in three-dimensional spheroid cultures of primary human hepatocytes, Clin. Pharmacol. Ther. 108 (2020) 844–855, doi:10.1002/cpt.1860.

[33] S. Ben-Moshe, Y. Shapira, A.E. Moor, R. Manco, T. Veg, K. Bahar Halpern, S. Itzkovitz, Spatial sorting enables comprehensive characterization of liver zonation, Nat. Metab. 1 (2019) 899–911, doi:10.1038/s42255-019-0109-9.

[34] C. Droin, J. El Kholtei, K. Bahar Halpern, C. Hurni, M. Rozenberg, S. Muvkadi, S. Itzkovitz, F. Naef, Space-time logic of liver gene expression at sub-lobular scale, Nat. Metab. 3 (2021) 43–58, doi:10.1038/s42255-020-00323-1.

[35] S. Yu, H. Wang, L. Yang, Y. Yan, Q. Cai, D. Ma, L. Jiang, Z. Gao, Z. Yu, Z. Xia, Spatial transcriptome profiling of normal human liver, Sci. Data. 9 (2022) 1–7, doi:10.1038/s41597-022-01676-w.

[36] J.A. Vale, A.T. Proudfoot, Paracetamol (acetaminophen) poisoning, Lancet 346 (1995) 547–552, doi:10.1016/S0140-6736(95)91385-8.

[37] M.M. Heldring, A.H. Shaw, J.B. Beltman, Unraveling the effect of intra- and intercellular processes on acetaminophen-induced liver injury, Npj Syst. Biol. Appl. 8 (2022), doi:10.1038/s41540-022-00238-5.

[38] G.H. Underhill, S.R. Khetani, Bioengineered liver models for drug testing and cell differentiation studies, Cell. Mol. Gastroenterol. Hepatol. 5 (2018) 426–439 e1, doi:10.1016/j.jcmgh.2017.11.012.

[39] T. Yoshikado, K. Toshimoto, T. Nakada, K. Ikejiri, H. Kusuhara, K. Maeda, Y. Sugiyama, Comparison of methods for estimating unbound intracellular-to-medium concentration ratios in rat and human hepatocytes using statinss, Drug Metab. Dispos. 45 (2017) 779–789, doi:10.1124/dmd.116.074823.

[40] C.C. Bell, V.M. Lauschke, S.U. Vorrink, H. Palmgren, R. Duffin, T.B. Andersson, M. Ingelman-Sundberg, Transcriptional, functional, and mechanistic comparisons of stem cell-derived hepatocytes, HepaRG cells, and three-dimensional human hepatocyte spheroids as predictive *in vitro* systems for drug-induced liver injury, Drug Metab. Dispos. 45 (2017) 419–429, doi:10.1124/dmd.116.074369.

[41] M. Schulz, A. Schmoldt, H. Andresen-Streichert, S. Iwersen-Bergmann, Revisited: therapeutic and toxic blood concentrations of more than 1100 drugs and other xenobiotics, Crit. Care. 24 (2020) 1–4, doi:10.1186/s13054-020-02915-5.

[42] I. Anundi, T. Lähteenmäki, M. Rundgren, P. Moldeus, K.O. Lindros, Zonation of acetaminophen metabolism and cytochrome P450 2E1-mediated toxicity studied in isolated periportal and perivenous hepatocytes, Biochem. Pharmacol. 45 (1993) 1251–1259, doi:10.1016/0006-2952(93)90277-4.

[43] P. An, L.L. Wei, S. Zhao, D.Y. Sverdlov, K.A. Vaid, M. Miyamoto, K. Kuramitsu, M. Lai, Y.V. Popov, Hepatocyte mitochondria-derived danger signals directly activate hepatic stellate cells and drive progression of liver fibrosis, Nat. Commun. (2020) 11, doi:10.1038/s41467-020-16092-0.

[44] K.E. Corey, R. Pitts, M. Lai, J. Loureiro, R. Masia, S.A. Osganian, J.L. Gustafson, M.M. Hutter, D.W. Gee, O.R. Meireles, E.R. Witkowski, S.M. Richards, J. Jacob, N. Finkel, D. Ngo, T.J. Wang, R.E. Gerszten, C. Ukomadu, L.L. Jennings, ADAMTSL2 protein and a soluble biomarker signature identify at-risk non-alcoholic steatohepatitis and fibrosis in adults with NAFLD, J. Hepatol. 76 (2022) 25–33, doi:10.1016/j.jhep.2021.09.026.

[45] M. Moreno-Torres, G. Quintás, J.V. Castell, The potential role of metabolomics in drug-induced liver injury (DILI) assessment, in: Metabolites, 2022, p. 12, doi:10.3390/metabo12060564.

[46] V.K. Verma, H. Li, R. Wang, P. Hirsova, M. Mushref, Y. Liu, S. Cao, P.C. Contreras, H. Malhi, P.S. Kamath, G.J. Gores, V.H. Shah, Alcohol stimulates macrophage activation through caspase-dependent hepatocyte derived release of CD40L containing extracellular vesicles, J. Hepatol. 64 (2016) 651–660, doi:10.1016/j.jhep.2015.11.020.

[47] B. Costa-Silva, N.M. Aiello, A.J. Ocean, S. Singh, H. Zhang, B.K. Thakur, A. Becker, A. Hoshino, M.T. Mark, H. Molina, J. Xiang, T. Zhang, T.M. Theilen, G. García-Santos, C. Williams, Y. Ararso, Y. Huang, G. Rodrigues, T.L. Shen, K.J. Labori, I.M.B. Lothe, E.H. Kure, J. Hernandez, A. Doussot, S.H. Ebbesen, P.M. Grandgenett, M.A. Hollingsworth, M. Jain, K. Mallya, S.K. Batra, W.R. Jarnagin, R.E. Schwartz, I. Matei, H. Peinado, B.Z. Stanger, J. Bromberg, D. Lyden, Pancreatic cancer exosomes initiate pre-metastatic niche formation in the liver, Nat. Cell Biol. 17 (2015) 816–826, doi:10.1038/ncb3169.

[48] L.C. Preiss, V.M. Lauschke, K. Georgi, C. Petersson, Multi-well array culture of primary human hepatocyte spheroids for clearance extrapolation of slowly metabolized compounds, AAPS J. 24 (2022) 1–12, doi:10.1208/s12248-022-00689-y.